Performance Evaluation of Millimeter-Wave Networks in the Context of Generalized Fading

Kibilda, J, Chun, YJ, Firyaguna, F, Yoo, SK, DaSilva, LA & Cotton, S

DOI 10.1109/glocomw.2018.8644492

Publisher: IEEE

Performance Evaluation of Millimeter-Wave Networks in the Context of Generalized Fading

Jacek Kibiłda*, Young Jin Chun†, Fadhil Firyaguna*, Seong Ki Yoo†, Luiz A. DaSilva*, and Simon L. Cotton†

*CONNECT, Trinity College, The University of Dublin, Ireland, E-mail: {kibildj,firyaguf,dasilval}@tcd.ie

†ECIT, Queen's University Belfast, UK, E-mail: {y.chun,sk.yoo,simon.cotton}@qub.ac.uk

***Abstract*—Building practical models of millimeter-wave networks which encompass every possible usage scenario presents a significant challenge. To address this issue, we propose an analytical framework based on stochastic geometry to model networks that are composed of millimeter-wave nodes. Our framework utilizes κ–μ shadowed fading to bring together, in a single model, various usage cases that span both indoor and outdoor environments. We analytically derive the distribution of the signal-to-interference-and-noise-ratio for a general millimeter-wave network distributed over a confined space. This allows us to explore the relationship between basic network parameters, such as node density, beamwidth, or transmit power, and the parameter space of the fading channel. Finally, we show, that when one assumes this network to be distributed over the whole Euclidean plane, its coverage can be described via remarkably simple closed-form expression.**

I. Introduction

One of the key promises of 5G systems is that they will deliver multigigabit per second speeds, using large swathes of bandwidth currently available in millimeter-wave (mmWave) spectrum bands around and above 30 GHz [1]. Thus, one of the challenges ahead for 5G is incorporating mmWave operating nodes in future network designs. This task will present significant challenges as the simple reuse of existing models developed for microwave frequencies is not sufficient to capture the performance characteristics of a network operating in one of the mmWave bands.

In particular, a new set of assumptions have to be made about the directionality of transmission/reception, the susceptibility of mmWave signals to blockages, increased path attenuation and weaker multi-path propagation effects [2], [3]. In the state of the art, the impact of these different factors on the performance of mmWave networks have been considered to a varying degree of accuracy in a combination of scenarios. For example, [4] studied the impact of highly directional antennas and beamforming, while [5] considered beam misalignments. Another feature that has received much research attention are blockages due to the fact that mmWave signals are highly attenuated by materials obstructing the direct path between the transmitter and receiver, causing significant disparity in power received via the line-of-sight (LOS) and non-LOS (NLOS) paths. One way to model these is to use multi-slope pathloss models with a number of degrees of freedom [6]. Yet, even relatively simple random blockage models can provide us with a reasonable level of accuracy [7]. Moreover one often considers additional randomly occurring blockage which is due to the user's body, which may decrease the power of the propagating mmWave signal by as much as 30–40 dB, e.g., [8]–[10].

While the above mentioned phenomena are considered essential for the performance analysis of mmWave networks, both large- and small-scale fading effects receive much less attention, and are either omitted (small-scale fading [2], large-scale fading [3]) or are modeled using idealized and perhaps not necessarily representative fading models, like the Rayleigh or Nakagami-m (see [11] and [3], [12], respectively). Under certain circumstances, small-scale fading may appear less pronounced in mmWave systems than in conventional systems [13] (due to directional transmissions and weak scattering). Yet, measurements across various propagation scenarios show that the strength of these effects varies with the type of environment and frequency (indoor environments and higher frequencies suffer more from shadow fading [14]), deployment (e.g., small-cell and device-to-device [15], [16]) or blockage condition considered (an LOS channel experiences different multi-path fading than NLOS channel [16]). Hence, these effects should be appropriately encapsulated in the overall channel model.

In this paper, we propose an analytical framework to evaluate the distribution function of the signal-to-noise and interference ratio (SINR) for general use case mmWave cellular networks. In order to generalize mmWave networks over a variety of usage cases we assume they operate over κ-μ shadowed fading channels. The strengths of κ-μ shadowed fading model lie in the physical interpretation of its parameters [17], good alignment with the measurements conducted for a number of communications scenarios (e.g., [18], [19]), as well as the fact that it generalizes popular fading distributions utilized in the literature, and captures large- and small-scale effects, such as human body shadowing.

In [20] a method was proposed to evaluate the average of an arbitrary function of the SINR under the κ–μ shadowed

This material is based in part upon work supported by the Science Foundation Ireland under grant 14/US/I3110 and the Department for Employment and Learning Northern Ireland under grant USI080.

fading. Herein we extend that method to find the distribution of the SINR of a mmWave network with a κ–μ shadowed fading channel in a closed-form. Furthermore, this distribution function renders itself in a succinct closed-form expression without any integral, for the case of a noise free environment with infinite plane interference. It is worth remarking that [21] relies on a similar strategy to find the distribution of the SINR, yet our results generalize this work by considering limitations to the considered area, as well as directionality of transmissions.

We observe that a mmWave network will have a finite density of mmWave nodes that can operate simultaneously and without coordination, while keeping interference at a level that does not severely degrade the network's performance. Furthermore, we verify that directional transmission is key to the operation of mmWave networks (achieving larger coverage), alongside the necessity of operation at high signal-to-noise ratios (SNRs) to enable NLOS transmission.

The remainder of this paper is organized as follows. In Section II we describe our mmWave network model. In Section III we provide our main analytical results, with sketches of the corresponding proofs to be found in the appendices. Finally, in Section IV we perform a numerical exploration of our model's parameter space, and in Section V we conclude and discuss follow up work.

II. System model

We consider a network in which wireless access points (in the following referred to as *nodes*) placement is modeled as a homogeneous Poisson point process (PPP) Φ with density $\lambda > 0$. We analyze the performance as seen from the perspective of the *reference user*, which represents an arbitrarily selected point on the Euclidean plane. Since Φ is stationary, without loss of generality we select a reference user at the origin. The reference user connects to the nearest transmitter node located within the network, thereby forming a *reference link*.

We assume all the signals that can reach the reference user come from nodes located within a fixed ball of radius ρ around the reference user, i.e., the considered network spans only a finite area. This allows us to represent both indoor and outdoor (small-cell) areas within a single model. This ball-area model is equivalent to the LOS blockage ball model, as presented in [4], [7], where the probability of having a direct link to a transmitter within radius ρ is 1, i.e., $p(d) = 1$ for $0 < d \leq \rho$, $p(d) = 0$ for $d > \rho$. As observed in [3], the impact of the transmitters for a large enough value of the radius may be ignored, leading to negligible errors in the analysis. We can always generalize our result to the entire Euclidean plane by setting $\rho \to \infty$, and as we shall see this case provides for a particularly attractive closed-form expression.

All the transmitters and receivers utilize directional transmission and reception, respectively. The directionality gain G_x between the transmitter in x and the reference user is determined via a sectored antenna pattern model, as described in [3]. This means that the total antenna gain is the product of the transmitter and receiver antenna gains, which in turn depend on the antenna alignment between the two. This makes the total gain a four-dimensional categorical random variable, with ν_j denoting the j-th possible alignment setting and η_j its probability. Following the cone-bulb model [10] and assuming normalized gains, we get that the main-lobe gain of the transmitter antenna is $(2\pi - g_b(2\pi - \omega_b))/\omega_b$, where ω_b is the width of the main-lobe and g_b is the side-lobe gain (the receiver antenna gain follows an analogous definition). Finally, we assume that each serving transmitter-receiver pair can adjust its antenna alignment, so that the reference link always operates at the maximum antenna array gain[1].
For the proposed model, the received SINR is given by

$$\mathrm{SINR} = \frac{\nu_1 H_{x_0} ||x_0||^{-\alpha}}{\sum_{x \in \Phi \setminus \{x_0\}} G_x H_x ||x||^{-\alpha} + \tau^{-1}}, \tag{1}$$

where τ denotes the ratio of the transmit power[2] to the noise power, ν_1 corresponds to the directionality gain between the serving transmitter and the receiver, α is the pathloss exponent of the power-law pathloss function (for simplicity we assume the intercept at the reference distance of 1 m to be unitary), and H_x denotes the power fading between the transmitter in x and the reference user.

We assume that the channel gain H is a random variable which follows the κ–μ shadowed distribution, whose probability density function (pdf) is given by

$$\begin{aligned} f_H(h) &= \frac{\theta_1^{m-\mu} h^{\mu-1}}{\theta_2^m \Gamma(\mu)} {}_1\mathrm{F}_1\left(m; \mu; \frac{\theta_2 - \theta_1}{\theta_2 \theta_1} h\right) \exp\left(-\frac{h}{\theta_1}\right) \\ &= \sum_{l=0}^{\infty} w_l \; f_Z(h; (l+\mu), \theta_1), \end{aligned} \tag{2}$$

where we use the series representation of the Hypergeometric function with the following notation

$$\theta_1 = \frac{\bar{\gamma}}{\mu(1+\kappa)}, \quad \theta_2 = \frac{(\mu\kappa + m)}{m}\theta_1,$$
$$w_l = \frac{(m)_l}{l!}\left(1 - \frac{\theta_1}{\theta_2}\right)^l \left(\frac{\theta_1}{\theta_2}\right)^m, \quad (m)_l = \frac{\Gamma(m+l)}{\Gamma(m)},$$

and $f_Z(h; (l+\mu), \theta_1)$ denotes the pdf of a Gamma-distributed random variable with parameters $l + \mu$ and θ_1 as follows

$$f_Z(z; (l+\mu), \theta_1) = \frac{1}{\theta_1^{l+\mu} \Gamma(l+\mu)} z^{l+\mu-1} \exp\left(-\frac{z}{\theta_1}\right). \tag{3}$$

One of the strengths of the κ-μ shadowed model lies in the physical interpretation of the four parameters (see, e.g., [18]). Namely: (i) κ describes the ratio of powers of the dominant component and scattered components (with $\kappa \to \infty$ corresponding to stronger dominant component), (ii) μ describes the number of scattering clusters in the environment (with large μ-value corresponding to a complex scattering environment), (iii) m describes the strength of the LOS shadowing (with $m \to 0$ corresponding to complete shadowing of the LOS component), and (iv) $\bar{\gamma}$ describes the average fading power.

[1]For analytical tractability, we ignored the effect of beam-misalignment and NLOS interference, which will be addressed in a future publication.

[2]For simplicity, we assume it is identical across all transmitters.

III. Analytical results

In the following we provide our main analytical results, which we deliver in two parts. First, we derive a closed-form expression for the complementary cumulative distribution function (ccdf) of SINR conditioned on the distance of the reference link. Then we provide the formula for the unconditional ccdf, presented in an integral form. Once we extend our area of interest to the entire Euclidean plane, this ccdf of the SINR can be provided in a remarkably attractive closed-form expression, given in the corollary.

Theorem 1: The conditional ccdf of the SINR for a link at distance r is given by

$$\begin{aligned}&\mathbb{P}\left(\text{SINR} > \zeta | R = r\right) = \\ &\mathcal{L}_{I+\tau^{-1}}\left(\frac{\zeta r^{\alpha}}{\nu_1 \theta_1}\right) \sum_{l=0}^{\infty} \sum_{n=0}^{l+\mu-1} \frac{w_l (-1)^n C_n(r)}{n!}, \\ &C_n(r) \triangleq \sum_{k=1}^{n} B_{n,k}(g^{(1)}(1), g^{(2)}(1), ..., g^{(n-k+1)}(1)),\end{aligned} \tag{4}$$

where $\mathcal{L}_{I+\tau^{-1}}(s) = \exp\left(-s/\tau\right)\mathcal{L}_I\left(s\right)$ and $g^{(k)}(1)$ are derived in Eq. (8) and Eq. (11), respectively, and $B_{n,k}$ denotes an ordinary Bell polynomial.

Proof: The sketch of a proof is given in Appendix A. ■

The (unconditional) ccdf of the SINR can be easily obtained by taking the expectation of Eq. (4) with respect to the reference link distance as follows

$$\begin{aligned}&\mathbb{P}\left(\text{SINR} > \zeta\right) = \mathbb{E}_R\left[\mathbb{P}\left(\text{SINR} > \zeta | R\right)\right] \\ &= \sum_{l=0}^{\infty} w_l \Bigg(\mathbb{E}_R\left[\mathcal{L}_I\left(\frac{\zeta R^{\alpha}}{\nu_1 \theta_1}\right)\right] + \\ &\sum_{n=1}^{l+\mu-1} \frac{(-1)^n}{n!} \mathbb{E}_R\left[\mathcal{L}_I\left(\frac{\zeta R^{\alpha}}{\nu_1 \theta_1}\right) C_n(R)\right]\Bigg).\end{aligned} \tag{5}$$

Corollary 1: The ccdf of the SINR for the infinite plane, i.e., as $\rho \to \infty$, is given by

$$\mathbb{P}\left(\text{SINR} > \zeta\right) = a_0^{-1} + \sum_{l=0}^{\infty} \sum_{n=1}^{l+\mu-1} \frac{w_l (-1)^n}{n!} C_n, \tag{6}$$

where C_n is given in Eq. (13), and a_0 in Eq. (14).

Proof: The sketch of a proof is given in Appendix B. ■

IV. Numerical results

In this section, we use the derived analytical formulas to numerically evaluate and compare the performance of mmWave systems for various propagation scenarios, i.e., different settings of the κ–μ shadowed fading model. In particular, we test for the impact of the direct path shadowing, small-scale fading, and the average SNR on the coverage performance. We consider the pathloss exponent of $\alpha_{\text{LOS}} = 2.1$ and $\alpha_{\text{NLOS}} = 4$ for the LOS and NLOS transmission, respectively.

Unless otherwise stated, we assume transmitter intensity of 0.01 nodes/m^2, and the area around the reference user of radius 10 m. We assume this area to always contain at least one transmitter, implying that the distribution of the reference link distance is conditioned on the event that the ball of radius ρ contains at least one point, which means it takes the form as derived in [22, Corollary 2.3]. Finally, we assume the transmitter antenna main-lobe beamwidth $\omega_b = 30\,^{\circ}$, side-lobe gain g_b = -10 dBm, and the average SNR of 10 dB. For ease of presentation, we assume the receiver antennas to be omnidirectional with unitary gains. Moreover, The LOS and NLOS transmissions are plotted using solid and dashed lines, respectively.

In Figs 1-4, we plot the coverage with respect to the node density where the coverage performance is divided by the vertical solid line into two regimes noise- and interference-limited. The noise-limited regime on the left-hand side corresponds to the case of a sparse network where the likelihood of the reference link being interfered by other nodes is relatively low. The interference-limited regime on the right-hand side corresponds to the case of a dense network where the interference from other nodes becomes the dominant factor affecting the performance. In the noise-limited regime, we observe that the coverage of the LOS link is significantly better than the NLOS case, whereas in the interference-limited regime, the opposite is true, i.e., the coverage of NLOS is better than the LOS case. This is due to the fact that the NLOS condition reduces the aggregated interference, achieving a higher SINR level for the interference-limited environment.

In Fig. 1, we notice that strong LOS shadowing has a profound effect on the coverage performance, degrading the coverage probability to values below 60% especially for the case of $m = 0.5$. In Fig. 2, we observe similar pattern as Fig. 1 where the cross-over point between the LOS and NLOS link shifts left towards lower node densities. If the network is operating at a higher SNR level, the aggregate interference can easily surpass the noise power, reaching interference-limited condition even at a low mmWave node density.

In Fig. 3 and Fig. 4, we observe that strong LOS component (large κ) and rich scattering environment with large number of multipath clusters (large μ) achieve better coverage performance. However, these improvements are relatively marginal, mostly due to the high directionality gains.

In Fig. 5 and Fig. 6, we notice that the coverage enhances by using beams with higher directional power concentration. The enhancement becomes nearly linear for the LOS link operating over high SNR. However, for propagation environments suffering strong LOS shadowing (low m), or operating in low SNR regime, or NLOS link, it is only beams with extremely narrow beamwidth ($< 50°$) that can provide reasonable coverage. Of course, the increasing gains of narrow-beam operation require perfect alignment between the beams of the receiver and mmWave node, as the errors in alignment may significantly diminish the performance gains [5].

Finally, in Fig. 7 and Fig. 8, we observe the behaviour of the ccdf of SINR for a mmWave network. This coverage performance is severely degraded by LOS shadowing (small m) or operation at an NLOS condition, but it can also be immediately improved by increasing the SNR level, which complies with our intuition.

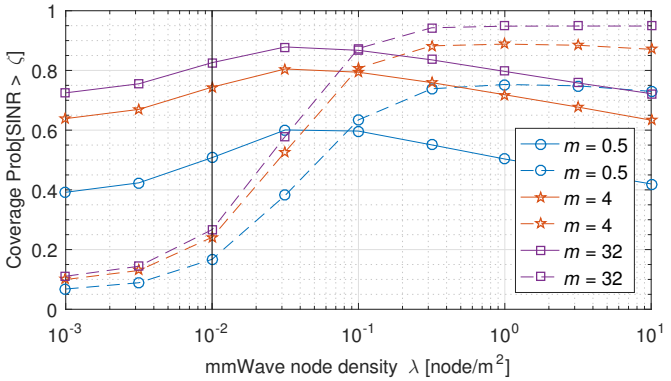

Fig. 1. Coverage probability versus mmWave node density for different m parameter with $\zeta = 0\,\text{dB}$, $\tau = 10\,\text{dB}$, $\kappa = 5$, $\mu = 1$, and $\bar{\gamma} = 1$.

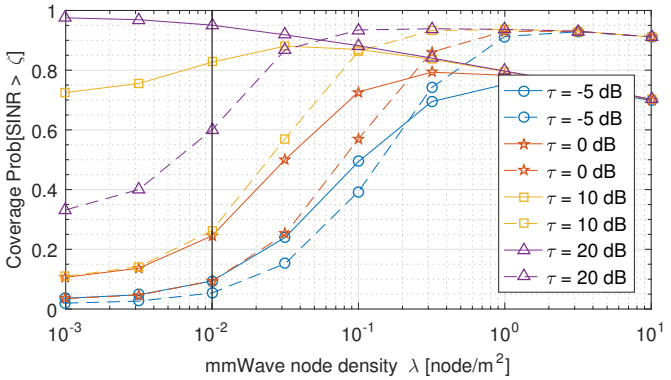

Fig. 2. Coverage probability versus mmWave node density for different τ parameter with $\zeta = 0\,\text{dB}$, $\kappa = 5$, $\mu = 1$, $m = 16$, and $\bar{\gamma} = 1$.

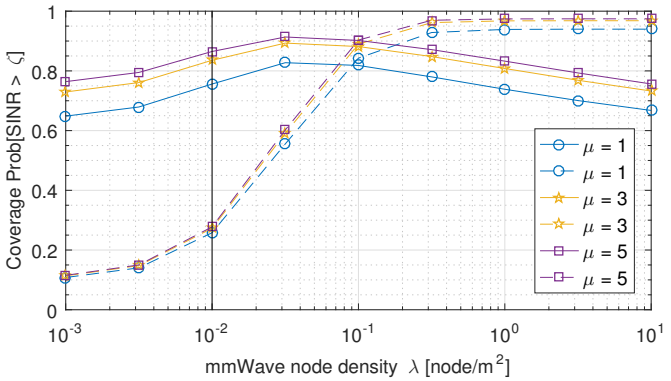

Fig. 3. Coverage probability versus mmWave node density for different μ parameter with $\zeta = 0\,\text{dB}$, $\tau = 10\,\text{dB}$, $\kappa = 5$, $m = 16$, and $\bar{\gamma} = 1$.

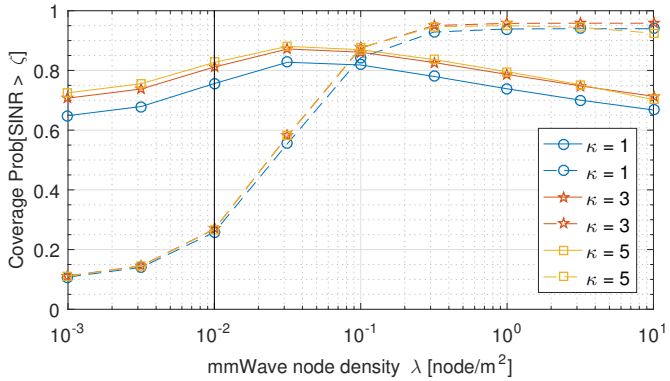

Fig. 4. Coverage probability versus mmWave node density for different κ parameter with $\zeta = 0\,\text{dB}$, $\tau = 10\,\text{dB}$, $\mu = 1$, $m = 16$, and $\bar{\gamma} = 1$.

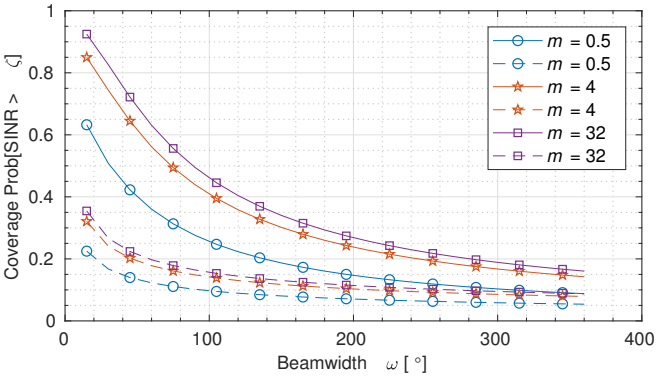

Fig. 5. Coverage probability versus beamwidth for different m parameter with $\zeta = 0\,\text{dB}$, $\tau = 10\,\text{dB}$, $\kappa = 5$, $\mu = 1$, and $\bar{\gamma} = 1$.

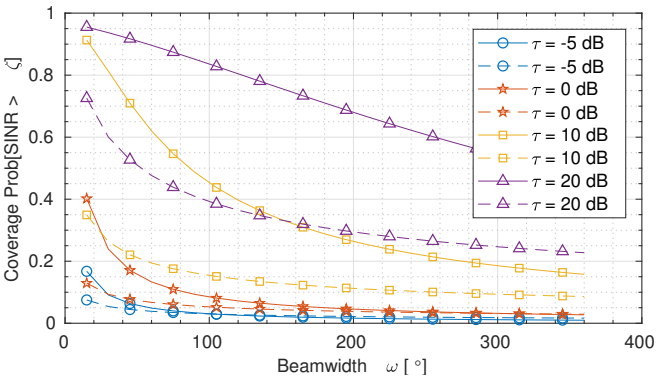

Fig. 6. Coverage probability versus beamwidth for different SNR values with $\zeta = 0\,\text{dB}$, $\kappa = 5$, $\mu = 1$, $m = 16$, and $\bar{\gamma} = 1$.

V. Conclusion

We have proposed an analytical framework using stochastic geometry to model and study networks complemented with mmWave operating nodes. Our model allows us to (1) derive the coverage probability of the general fading channel, e.g., κ-μ shadowed fading, in closed-form that does not require integral, (2) find the density of mmWave nodes that can operate simultaneously and without coordination, and (3) show the importance of directional transmission for the operation of a mmWave network (allowing for much increased coverage), and the necessity of operation at high SNRs to enable NLOS transmission.

The model and study presented here are really just an opening into the performance analysis of mmWave networks in the context of generalized fading. Using the obtained model will allow us to consider design aspects for a variety of 5G use cases, such as device-to-device, or indoor hotspot, which we can populate with real-life measurements, while accounting for mixed LOS/NLOS environments. Furthermore, the analytical extensions could possibly involve more general node placement models, such as in [23], and addressing the computational complexity of Bell polynomials.

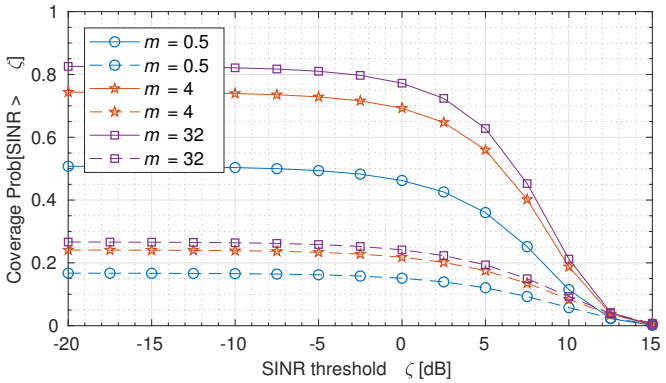

Fig. 7. Coverage probability versus SINR threshold ζ for different m parameter with $\tau = 10\,\text{dB}$, $\kappa = 5$, $\mu = 1$, and $\bar{\gamma} = 1$.

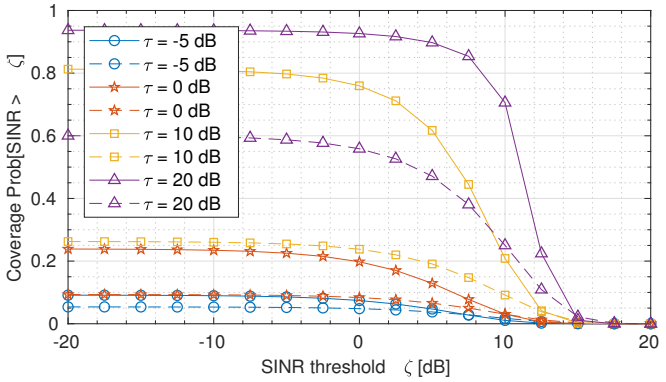

Fig. 8. Coverage probability versus SINR threshold ζ for different τ parameter with $\kappa = 5$, $\mu = 1$, $m = 16$, and $\bar{\gamma} = 1$.

Appendix A
Sketch of a Proof of Theorem 1

The coverage probability of a cellular network can be defined for a given threshold ζ as

$$\begin{aligned}\mathbb{P}\left(\text{SINR} > \zeta\right) &= \mathbb{P}\left(H > \frac{\zeta R^{\alpha}\left(I+\tau^{-1}\right)}{\nu_1\theta_1}\right)\\ &\overset{(a)}{=} \mathbb{E}\left[\bar{F}_H\left(\frac{\zeta R^{\alpha}\left(I+\tau^{-1}\right)}{\nu_1\theta_1}\right)\right]\\ &\overset{(b)}{=} \sum_{l=0}^{\infty}\sum_{n=0}^{l+\mu-1}\frac{w_l}{n!}\mathbb{E}\left[t^n\exp\left(-t\right)\right]\\ &\overset{(c)}{=} \sum_{l=0}^{\infty}\sum_{n=0}^{l+\mu-1}\frac{w_l(-1)^n}{n!}\frac{\mathrm{d}^n\mathcal{L}_t(s)}{\mathrm{d}s^n}\bigg|_{s=1},\end{aligned} \tag{7}$$

where ζ is the SINR threshold and I is the interference; (a) $\bar{F}_H(\cdot)$ is the ccdf of the fading random variable; (b) comes from representing the ccdf of the power fading using Eq. (2), with μ for the serving mmWave node assumed to be integer (for non-integer values of μ we can use the approximation provided in [21]) and $t = \frac{\zeta r^{\alpha}}{\nu_1\theta_1}\left(I+\tau^{-1}\right)$; (c) $\mathcal{L}_t(s) = \exp\left(-s\frac{\zeta r^{\alpha}}{\nu_1\tau\theta_1}\right)\mathcal{L}_I\left(s\frac{\zeta r^{\alpha}}{\nu_1\theta_1}\right)$, where $\mathcal{L}_I(\cdot)$ is the Laplace transform of the aggregate interference.

The Laplace transform of the interference can be derived as

$$\begin{aligned}\mathcal{L}_I\left(s\right) &= \exp\left(-2\pi\lambda\int_r^{\rho}\left(1-\mathbb{E}_{H,G}\left[\mathrm{e}^{-sGHu^{-\alpha}}\right]\right)u\,\mathrm{d}u\right)\\ &= \exp\left(-\pi\lambda\left(\rho^2-r^2\right)\right)\exp\Bigg(-\pi\lambda\sum_{l=0}^{\infty}w_l\\ &\sum_{j=1}^{4}\eta_j\Big(r^2{}_2\mathrm{F}_1(l+\mu,-\delta;1-\delta;-sr^{-\alpha}\nu_j\theta_1)+\\ &-\rho^2{}_2\mathrm{F}_1(l+\mu,-\delta;1-\delta;-s\rho^{-\alpha}\nu_j\theta_1)\Big)\Bigg).\end{aligned} \tag{8}$$

Then, let us express $\exp\left(-s\frac{\zeta r^{\alpha}}{\nu_1\tau\theta_1}\right)\mathcal{L}_I\left(s\frac{\zeta r^{\alpha}}{\nu_1\theta_1}\right)$ as a composite function $\exp\left(g(s)\right)$, where $g(s)$ denotes the following

$$\begin{aligned}g(s) &= -\frac{\zeta r^{\alpha}s}{\theta_1\tau\nu_1}-\pi\lambda\left(\rho^2-r^2\right)-\pi\lambda\sum_{l=0}^{\infty}w_l\sum_{j=1}^{4}\eta_j\\ &\times\Bigg(r^2{}_2\mathrm{F}_1(l+\mu,-\delta;1-\delta;-s\bar{\nu}_j\zeta)-\\ &\rho^2{}_2\mathrm{F}_1(l+\mu,-\delta;1-\delta;-s\bar{\nu}_j\zeta(r/\rho)^{\alpha})\Bigg),\end{aligned} \tag{9}$$

where $\bar{\nu}_j = \nu_j/\nu_1$. Now, we use the following version of the Faa di Bruno formula to evaluate the derivative term in Eq. (7)

$$\frac{\mathrm{d}^n f(g(s))}{\mathrm{d}x^n} = \sum_{k=1}^{n} f^{(k)}(g(s))B_{n,k}(g'(s),\ldots,g^{(n-k+1)}(s)). \tag{10}$$

It is obvious that $f^{(k)}\left(g(s)\right) = f\left(g(s)\right) = \exp\left(g(s)\right)$, while the k-th order derivative of $g(s)$ can be found using the properties of the Gauss Hypergeometric function [24]

$$\begin{aligned}g^{(k)}(1) &= \mathbb{1}_{[k=1]}\left(-\frac{\zeta r^{\alpha}}{\theta_1\tau\nu_1}\right)+r^2\pi\lambda a_k,\\ a_k &= \frac{(-\zeta)^k\,\delta}{k-\delta}\sum_{l=0}^{\infty}w_l(l+\mu)_k\times\\ &\sum_{j=1}^{4}\eta_j(\bar{\nu}_j)^k\Bigg({}_2\mathrm{F}_1(l+\mu+k,k-\delta;k+1-\delta;-\zeta\bar{\nu}_j)-\\ &\left(\frac{\rho}{r}\right)^{2-\alpha k}{}_2\mathrm{F}_1(l+\mu+k,k-\delta;k+1-\delta;-\zeta\bar{\nu}_j(r/\rho)^{\alpha})\Bigg).\end{aligned} \tag{11}$$

Now, putting all the pieces together we get the conditional coverage probability expression in Eq. (4).

Appendix B
Proof of Corollary 1

We can derive the expectations in Eq. (5) as follows

$$\mathbb{E}_R\left[\mathcal{L}_I\left(\frac{\zeta R^{\alpha}}{\theta_1\nu_1}\right)\right] = \int_0^{\infty}2\pi\lambda r\mathrm{e}^{-r^2\pi\lambda a_0}\,\mathrm{d}r = \frac{1}{a_0}, \tag{12}$$

$$\mathbb{E}_R\left[\mathcal{L}_I\left(\frac{\zeta R^{\alpha}}{\theta_1\nu_1}\right)C_n(R)\right]$$
$$\overset{(a)}{=}\sum_{k=1}^{n}B_{n,k}(a_1,\ldots,a_{n-k+1})\int_0^{\infty}2\pi\lambda r\mathrm{e}^{-r^2\pi\lambda a_0}\left(r^2\pi\lambda\right)^k\mathrm{d}r$$
$$=\sum_{k=1}^{n}\frac{B_{n,k}(a_1,\ldots,a_{n-k+1})\Gamma\left(k+1\right)}{a_0^{k+1}}\triangleq C_n, \tag{13}$$

where we utilize the fact that for an infinite plane PPP the reference link distance distribution follows [22, Corollary 2.4], and (a) can be obtained by taking out $(r^2\pi\lambda)^k$ from the Bell polynomial terms and noticing that the Laplace transform simplifies to $\exp\left(\pi\lambda r^2(1-a_0)\right)$ with

$$a_k=\frac{(-\zeta)^k\,\delta}{k-\delta}\sum_{l=0}^{\infty}w_l\cdot(l+\mu)_k\times$$
$$\sum_{j=1}^{4}\eta_j(\bar{\nu}_j)^k{}_2\mathrm{F}_1(l+\mu+k,k-\delta;k+1-\delta;-\bar{\nu}_j\zeta). \tag{14}$$

This concludes the proof.

REFERENCES

[1] P. Nikolich *et al.*, "Standards for 5G and Beyond: Their Use Cases and Applications," *IEEE 5G Tech Focus*, vol. 1, no. 2, June 2017. [Online]. Available: https://5g.ieee.org/tech-focus/june-2017/standards-for-5g-and-beyond

[2] M. Di Renzo, "Stochastic geometry modeling and analysis of multi-tier millimeter wave cellular networks," *IEEE Transactions on Wireless Communications*, vol. 14, no. 9, pp. 5038–5057, Sep. 2015.

[3] J. G. Andrews *et al.*, "Modeling and analyzing millimeter wave cellular systems," *IEEE Transactions on Communications*, vol. 65, no. 1, pp. 403–430, Jan. 2017.

[4] X. Yu *et al.*, "Coverage analysis for millimeter wave networks: The impact of directional antenna arrays," *IEEE Journal on Selected Areas in Communications*, vol. 35, no. 7, pp. 1498–1512, July 2017.

[5] M. Rebato *et al.*, "Stochastic geometric coverage analysis in mmWave cellular networks with a realistic channel model," *IEEE Global Communications Conference (Globecom)*, Dec. 2017.

[6] "5G Channel Model for bands up to 100 GHz," mmWaveMagic, Tech. Rep. 2.3, Oct. 2016. [Online]. Available: http://www.5gworkshops.com/5GCM.html

[7] T. Bai and R. W. Heath, "Coverage and rate analysis for millimeter-wave cellular networks," *IEEE Transactions on Wireless Communications*, vol. 14, no. 2, pp. 1100–1114, Feb. 2015.

[8] ——, "Analysis of self-body blocking effects in millimeter wave cellular networks," in *Asilomar Conference on Signals, Systems and Computers*, Nov. 2014, pp. 1921–1925.

[9] M. N. Kulkarni *et al.*, "Impact of Humans on the Design and Performance of Millimeter Wave Cellular Networks in Stadiums," in *IEEE Wireless Communications and Networking Conference (WCNC)*, Mar. 2017, pp. 1–6.

[10] F. Firyaguna *et al.*, "Coverage and Spectral Efficiency of Indoor mmWave Networks with Ceiling-Mounted Access Points," in *IEEE Global Communications Conference (Globecom)*, Dec. 2017.

[11] A. K. Gupta, J. G. Andrews, and R. W. Heath, "On the Feasibility of Sharing Spectrum Licenses in mmWave Cellular Systems," *IEEE Transactions on Communications*, vol. 64, no. 9, pp. 3981–3995, Sep. 2016.

[12] E. Turgut and M. C. Gursoy, "Coverage in heterogeneous downlink millimeter wave cellular networks," *IEEE Transactions on Communications*, vol. 65, no. 10, pp. 4463–4477, Oct. 2017.

[13] T. S. Rappaport *et al.*, "Millimeter Wave Mobile Communications for 5G Cellular: It Will Work!" *IEEE Access*, vol. 1, pp. 335–349, 2013.

[14] G. R. Maccartney *et al.*, "Indoor office wideband millimeter-wave propagation measurements and channel models at 28 and 73 ghz for ultra-dense 5g wireless networks," *IEEE Access*, vol. 3, pp. 2388–2424, 2015.

[15] S. K. Yoo *et al.*, "Measurements of the 60 GHz UE to eNB Channel for Small Cell Deployments," *IEEE Wireless Communications Letters*, vol. 6, no. 2, pp. 178–181, Apr. 2017.

[16] ——, "Channel Characteristics of Dynamic Off-Body Communications at 60 GHz under Line-of-Sight (LOS) and Non-LOS Conditions," *IEEE Antennas and Wireless Propagation Letters*, vol. 16, pp. 1553–1556, Feb. 2017.

[17] J. F. Paris, "Statistical Characterization of κ–μ Shadowed Fading," *IEEE Transactions on Vehicular Technology*, vol. 63, no. 2, pp. 518–526, Feb. 2014.

[18] S. L. Cotton, "Human body shadowing in cellular device-to-device communications: channel modeling using the shadowed κ-μ fading model," *IEEE Journal on Selected Areas in Communications*, vol. 33, no. 1, pp. 111–119, Jan. 2015.

[19] S. K. Yoo *et al.*, "The κ-μ/inverse gamma and η-μ/inverse gamma composite fading models: Fundamental statistics and empirical validation," *IEEE Transactions on Communications*, 2018.

[20] Y. J. Chun *et al.*, "A Comprehensive Analysis of 5G Heterogeneous Cellular Systems Operating Over κ–μ Shadowed Fading Channels," *IEEE Transactions on Wireless Communications*, vol. 16, no. 11, pp. 6995–7010, Nov. 2017.

[21] S. Parthasarathy and R. K. Ganti, "Coverage Analysis in Downlink Poisson Cellular Network With κ–μ Shadowed Fading," *IEEE Wireless Communications Letters*, vol. 6, no. 1, pp. 10–13, Feb. 2017.

[22] S. Srinivasa and M. Haenggi, "Distance distributions in finite uniformly random networks: Theory and applications," *IEEE Transactions on Vehicular Technology*, vol. 59, no. 2, pp. 940–949, Feb. 2010.

[23] C. Saha, M. Afshang, and H. S. Dhillon, "3GPP-inspired HetNet model using Poisson cluster process: Sum-product functionals and downlink coverage," *IEEE Transactions on Communications*, 2017.

[24] I. Charpentier, C. Dal Cappello, and J. Utke, "Efficient higher-order derivatives of the hypergeometric function," in *Advances in Automatic Differentiation*. Springer, 2008, pp. 127–137.